Radiation asymmetry in JET disruption mitigation experiments with shattered pellet injection

OPEN ACCESS
IOP Publishing
Plasma Physics and Controlled Fusion
Plasma Phys. Control. Fusion **66** (2024) 085007 (9pp)
https://doi.org/10.1088/1361-6587/ad5933

Radiation asymmetry in JET disruption mitigation experiments with shattered pellet injection

L Piron[1,2,*], S Jachmich[3], L Baylor[4], M Baruzzo[5], M Lehnen[3], P Carvalho[6], M Kong[7], P Martin[1,2], T Lo Presti Piccolo[1], S Silburn[6], D Terranova[2,8], D Valcarcel[6], JET Contributors[9] and Eurofusion Tokamak Exploitation Team[10]

[1] Department of Physics and Astronomy, University of Padova, Padova, Italy
[2] Consorzio RFX (CNR, ENEA, INFN, Università di Padova, Acciaierie Venete SpA), C.so Stati Uniti 4, 35127 Padova, Italy
[3] ITER Organization, Route de Vinon-sur-Verdon, CS 90 046, 13067 St. Paul Lez Durance, Cedex, France
[4] Oak Ridge National Laboratory, Oak Ridge, TN, United States of America
[5] ENEA, Fusion and Nuclear Safety Department, C.R. Frascati, Rome, Italy
[6] CCFE, Culham Science Centre, Abingdon OX14 3DB, United Kingdom
[7] École Polytechnique Fédérale de Lausanne (EPFL), Swiss Plasma Center (SPC), CH-1015 Lausanne, Switzerland
[8] Istituto per la Scienza e la Tecnologia dei Plasmi, CNR, Padova, Italy

E-mail: lidia.piron@unipd.it

Received 25 March 2024, revised 16 May 2024
Accepted for publication 17 June 2024
Published 27 June 2024

Abstract

In ITER, to mitigate the deleterious effects of plasma disruptions, massive quantities of radiating impurities will be injected into the disrupting plasma by shattered pellet injectors (SPI) to pre-emptively radiate away the stored thermal and magnetic energy (Lehnen *et al Proc. 27th IAEA Fusion Energy Conf. (FEC 2018) (Gandhinagar, India)* EX/P7-12). However, asymmetries in the radiation pattern could result in intense photon flashes during the thermal quench that could locally damage or erode the stainless steel plasma-facing surface of the diagnostic port plugs (Pitts *et al* 2015 *J. Nucl. Mater.* **463** 748–75). Experiments have been undertaken at JET to assess the potential dependence of the radiated power asymmetry on plasma energy during SPI mitigated disruptions. Calculations of the toroidal asymmetry in the

[9] See Maggi *et al* 2024 (https://doi.org/10.1088/1741-4326/ad3e16) for JET Contributors.
[10] See the author list of 'Progress on an exhaust solution for a reactor using EUROfusion multi-machines capabilities' by E Joffrin *et al* to be published in *Nuclear Fusion Special Issue: Overview and Summary Papers from the 29th Fusion Energy Conference (London, UK, 16–21 2023).*
[*] Author to whom any correspondence should be addressed.

radiated power indicate that the toroidal peaking factor is largest near the SPI position and decreases with the plasma stored energy, which is a promising result in view of radiation heat loads during mitigated disruptions in ITER.

Keywords: JET, plasma, SPI control, radiation

1. Introduction

A disruption mitigation system (DMS) is essential for ensuring reliable and successful operation of ITER from the first experimental campaign onwards by minimizing the potential damage to the machine during disruptions. During a disruption event, in the thermal quench phase, the rapid loss of thermal energy has the potential to cause surface melting of plasma-facing components and the high electromagnetic loads arising from eddy and halo currents in the in-vessel components can be close to the design limits. The induced Dreicer electric field can accelerate electrons, which become runaway electrons (RE) that are able to deposit their energy, a significant fraction of the stored magnetic energy, in localized regions of the bulk material, causing water leaks [1, 2].

For disruption avoidance, the ITER plasma control system will monitor a chain of events preceding the disruption and will trigger an appropriate control response, aiming to either completely restore the standard plasma parameters within the predetermined operational range or, in extreme cases, safely terminate the plasma. However, achieving 100% reliability in avoiding disruptions is not guaranteed. If restoring a stable plasma scenario becomes impossible, the DMS will be required to intervene [3].

The current disruption mitigation strategy envisioned for ITER relies on converting plasma energy into line radiation by rapidly injecting neon together with protium to increase the plasma density. This dual objective aims to dissipate energy, thereby decreasing thermal loads on the ITER tokamak components. Simultaneously, the density increase serves to prevent or mitigate the generation of RE by minimizing the processes associated with RE generation and avalanche.

The method adopted to dissipate the plasma energy and to increase the plasma density consists of injecting massive amounts of impurities, fuel, or both into the plasma in the form of fragmented cryogenic pellets using the Shattered Pellet Injection (SPI) system [4–7].

Several devices, such as AUG [8], DIII-D [9], JET [6], KSTAR [10] J-TEXT [11] and HL-2 A [12], have contributed towards the definition of the DMS in ITER thanks to the installation and operation of SPI systems. Useful lessons have been learned in firing of the pellets to remove efficiently the thermal energy and to dissipate REs.

In particular, at JET we investigated how symmetrically the energy is radiated around the torus during SPI mitigated disruptions. This study is of particular importance, because it is expected in ITER that about 80% of the total stored thermal energy is lost during the thermal quench. Therefore, in cases where the radiated power is high, asymmetries in the radiation pattern could potentially cause damage or erosion to stainless steel plasma-facing surfaces of the diagnostic port plugs [13–15].

The radiation asymmetries can be characterized by a poloidal and toroidal peaking factor, i.e. PPF and TPF respectively, which is defined as the ratio of the maximum radiated power to the mean radiated power in the direction of interest.

Although ITER is considering to change the main chamber first wall material from beryllium to tungsten, potential heat flux resulting from high local radiation power is still a concern for the stainless steel components [14].

In this context, an assessment of the potential dependence of the radiated power asymmetry in the toroidal direction on plasma energy has been conducted at the JET tokamak. JET was the suitable device for this study since it was equipped with a bolometry system and error field correction coils (EFCCs) [16], which can induce an $n = 1$ magnetic island that effects the radiation asymmetry during the thermal quench [6, 7, 17, 18].

In this manuscript, section 2 details the experimental setup and the methodology adopted for investigating radiation asymmetry at JET. Section 3 presents the experimental results covering a range of different plasma stored energy. Section 4 summaries the findings and provides some conclusions.

2. Experimental setup

At JET, the SPI system consists of a three barrel pellet gun, which is mounted on top of the machine, as shown in the sketch reported in figure 1(a), between octants 1 and 2 [4]. The barrels have different diameters and allow the desublimation of protium, deuterium (D_2), neon and mixtures of these gases.

In the experiments analyzed here, 8.1 mm diameter and 13 mm long pellet made of Neon/Deuterium ∼81% has been used, where the percentage of Neon mixed into Deuterium is defined as the ratio of Neon atoms to the total number of atoms in the pellet, including the Deuterium shell ($\sim 2.3 \times 10^{22}/5.8 \times 10^{21}$ Neon/Deuterium atoms).

The pellets, after being dislodged and accelerated by a pure D_2 gas pulse, pass through a microwave cavity diagnostic [19], which allows the characterization of the pellet integrity, mass and velocity. Recently, the SPI has been modified to better control the pellet velocity. In this study, two different pellet velocities have been used, i.e. the slow one ∼180 m s^{-1} and the fast one ∼320 m s^{-1}, to analyze its impact on radiation asymmetry.

After a travel time of 15–26 ms, the pellets are shattered by impacting on a S-bend tube inside the vacuum vessel just above the plasma [4]. The arrival time of the fragments in the plasma has been inferred from data of a fast camera which

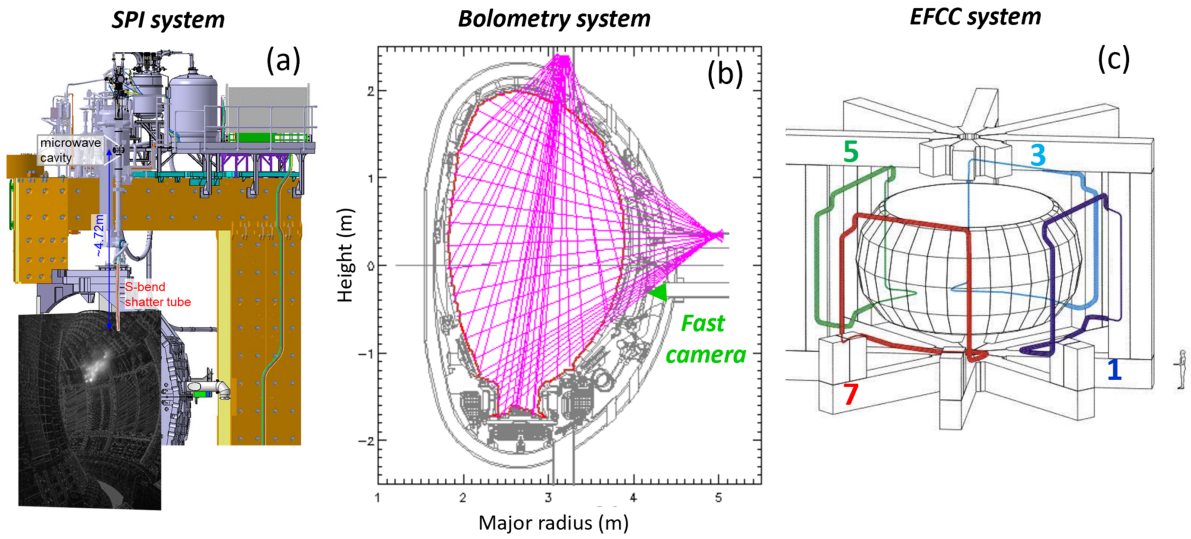

Figure 1. Overview of JET systems exploited for radiation asymmetry studies: (a) the shattered pellet injector located between octants 1 and 2, at $\phi = 11.25°$, on one of the vessel's vertical ports, (b) the bolometry system to measure radiation during the shattered pellet injection activation, with the corresponding 24 vertical and horizontal line of sights from two arrays, located in octants 3 and 6, at $\phi = 90°$ and $\phi = 225°$ respectively, together with the position of the fast camera used to check the fragment arrival, and (c) the error field correction system, consisting of four coils positioned external to the vacuum vessel in octants 1, 3, 5 and 7.

views the injection location tangentially (see example snapshot in figure 1(a)). A potential premature breakage, after the pellet has passed the microwave cavity diagnostic and before the shatter section, can be determined from these fast camera observations at the injection point.

The radiation properties during radiated asymmetry studies have been investigated analyzing measurements from vertical and horizontal bolometer arrays, made up of 24 lines of sight each and with distinct geometries, as shown in figure 1(b), which are located at are 90° and 225° toroidally, respectively. The total radiated power is computed for each location from a weighted sum across the poloidal cross-section and has been cross-calibrated prior the disruption assuming toroidal uniformity. The coverage the divertor region slightly differs and can result in different radiated power for configurations in which divertor radiation dominates. However, during disruptions in particular induced by SPI, radiation in the main chamber is the predominant contribution, while that from the divertor can be neglected [20].

It is worth anticipating that bolometry signals have also been analyzed to detect potential broken pellets. This analysis complements the information obtained from the microwave cavity and fast camera data. The evaluation of pellet integrity, using data from multiple diagnostics, holds particular significance in radiation asymmetry studies. This approach helps eliminate potential outliers in the database, which could otherwise impact the calculation of the TPF, the quantity of interest in this paper.

EFCC system sketched in figure 1(c), originally designed to correct intrinsic error fields, has been also exploited in this study to induce an $n = 1$ magnetic field perturbation whose direction can be tailored by changing the polarity of the EFCC current. By applying this external field perturbation, the toroidal O-point location of the $n = 1$ locked mode can be imposed. 3D MHD modelling indeed shows that the phase of the $n = 1$ magnetic island together with the particular distribution of the injected gas determines the radiation peaking and the associated heat loads [17, 21]. This prediction has been confirmed by experimental results in several devices, i.e. Alcator C-Mod [22], DIII-D [8, 18] and JET [6, 7].

The external $n = 1$ field perturbation has been applied prior to the firing of the SPI, during the plasma steady-state phase, as shown in figure 2(a). Similarly to [6, 7], the current polarity in the 4 EFCCs has been changed on a shot to shot basis to acquire radiation power from different toroidal locations. The variation of the measured radiated power at two toroidal locations can then be used to determine the TPF while the location of the $n = 1$ magnetic island has been derived from the magnetic measurements using set of orthogonal saddle coils, located external to the vacuum vessel, which have been compensated by the external magnetic field perturbation as in [16].

In earlier investigations [6], the radiation asymmetry has been investigated in a scenario characterized by a 2.0 MA plasma current (I_p), 2.5 T toroidal magnetic field (B_t) and heated by 13 MW NBI power. In this work, the analysis has been extended using the same experimental procedure, but in a pure Ohmic plasma or with an additional 20 MW NBI power. The goal is to explore potential correlations between the radiation asymmetry and the plasma energy.

Figure 2 shows typical discharges of the three types of target plasmas for which this study has been carried out. In all these plasmas, the same SPI pellet compositions have been used, i.e. 8.1 mm pellet from barrel B, made up of ~81% Neon and injected at around 180 m s^{-1}. As can be inferred from figure 2(c), the stored energy changes from 0.4 MJ to 3.2 MJ with increasing NBI power from 0 to around 20 MW.

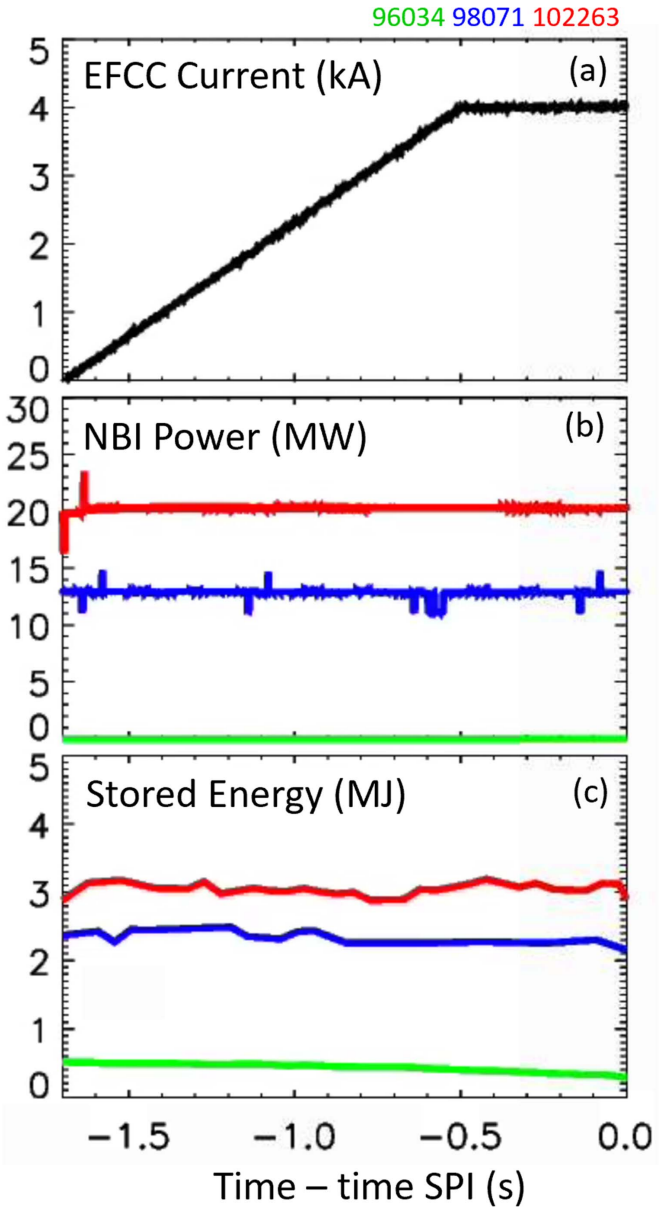

Figure 2. Time behavior of (a) EFCC current, (b) NBI power and (c) stored energy in $I_p = 2$ MA, $B_t = 2.5$ T discharges, where SPI has been fired for radiation asymmetry studies in plasmas with different plasma energy levels.

3. Experimental results of radiation asymmetry during SPI and the interpretative modelling

To assess radiation asymmetry, it is essential to have either comprehensive toroidal coverage with bolometry diagnostics or to deduce the toroidal distribution from the variation in radiated power measured at a specific toroidal position relative to the magnetic island phase. As mentioned earlier, at JET, the latter method has been employed by inducing external magnetic perturbations through EFCCs.

The radiation asymmetry can be characterized by the asymmetry factor that is defined as the difference between the vertical and the horizontal radiated power divided by their sum, i.e.

$$\Delta P/\sum \mathrm{P} = \left(\mathrm{P_{rad}}^{\mathrm{Vert}} - \mathrm{P_{rad}}^{\mathrm{Hor}}\right) / \left(\mathrm{P_{rad}}^{\mathrm{Vert}} + \mathrm{P_{rad}}^{\mathrm{Hor}}\right). \quad (1)$$

This quantity has been calculated during the thermal quench at the time when the radiation is maximum.

This asymmetry factor cannot be directly converted into a TPF. Nevertheless, the data can be interpreted by assuming a cosine-like radiation distribution driven by the $n = 1$ mode and a Gaussian-type toroidal distribution of the impurity density as in [6, 7].

The disruption mitigation properties, as the radiation asymmetries, can change in case the injection is prolonged due to a broken pellet. To correctly retrieve the TFP, it is of paramount importance to identify in the database and discard from the analysis those discharges where the pellets arrived broken already at the microwave cavity or before arriving to the funnel and the S bend in the shatter tube.

Three distinct pellet behaviors were observed during the analysis and have been defined based on microwave, bolometry, and fast camera data.

Figure 3 illustrates these pellet behaviors as examples. The data refers to discharges #102248 (intact pellet), #102911 (broken pellet when passing through the microwave cavity), #102547 (broken pellet before the funnel and S-tube). These discharges have $I_p = 2$ MA, $B_t = 2.5$ T and 3.2 MJ plasma stored energy. The injected pellet had the same composition (8.1 mm diameter and 13 mm long, made of Neon/Deuterium ~81%), but the injection velocity was different: in #102248 it was 180 m s^{-1}, while in #102911 and #102547, it was 320 m s^{-1}.

The behavior of plasma current, the loop voltage and the induced $n = 1$ B_r amplitude around the disruption time are reported in panels (a), (g), (m), (b), (h), (n), (c), (i), (o), respectively.

In the following, we described in details the three distinct pellet behaviors.

(i) #102248, reported on the left panels of figure 3, represents the ideal case where the pellet arrives intact at the shatter tube. Indeed a single spike is present in the microwave cavity, as shown in figure 3(d), and noticeable sharp increase of radiation can be seen in both the vertical and horizontal bolometry signals, reported in figure 3(e). The arrival of an intact pellet appears as a single plume pattern in fast cameras, as depicted in figure 3(f) which is a fast camera imaging taken at $t = 15.975$ s.

(ii) #102911, on the panels in the center of figure 3, represents a case with broken pellet when passing the microwave cavity. Indeed, the microwave cavity signal, reported in panel (*j*), shows two spikes, and the vertical P_{rad} signal in panel (*m*) instead of having a sharp spike, it is characterized by a slight rising phase, at around $t = 15.978$ s, followed by a spike in radiation. This pattern is distinctive trait of a broken pellet. To quantify the contribution

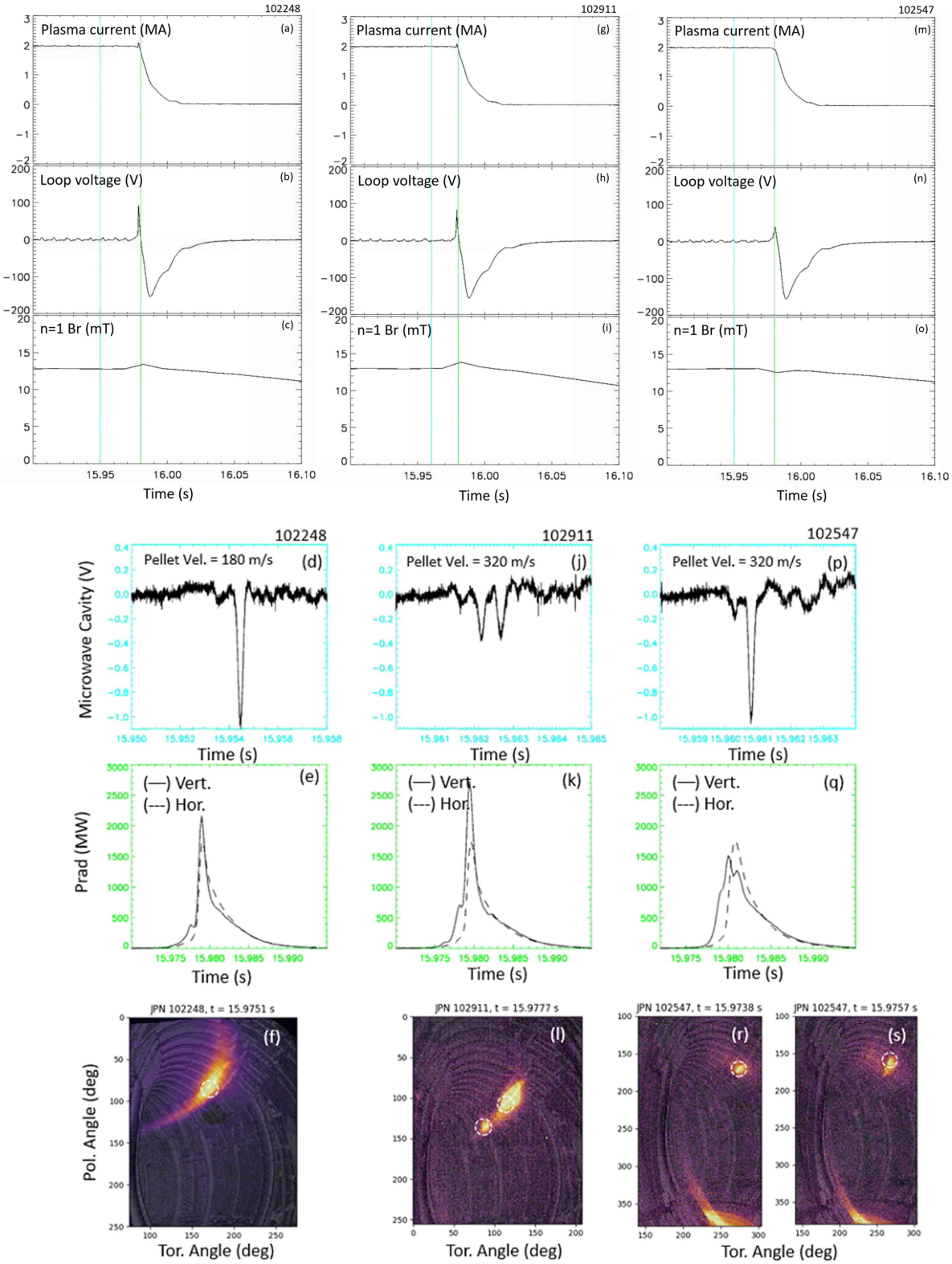

Figure 3. Time behavior of (a), (g), (m) plasma current, (b), (h), (n) toroidal voltage, (c), (i), (o) $n = 1$ Br amplitude, (d), (j), (p) microwave cavity signal, (e), (k), (q) radiated power measured by the vertical (solid lines) and horizontal (dashed line) bolometer and (f), (l), (r), (s) fast camera images of the pellet arrival in the vacuum chamber. Data refers to 2 MA plasma current, 2.5 T toroidal magnetic field plasmas where SPI has been fired for radiation asymmetry studies. The vertical cyan line indicates when the pellet passed through the microwave cavity, while the green one when it arrives in the plasma.

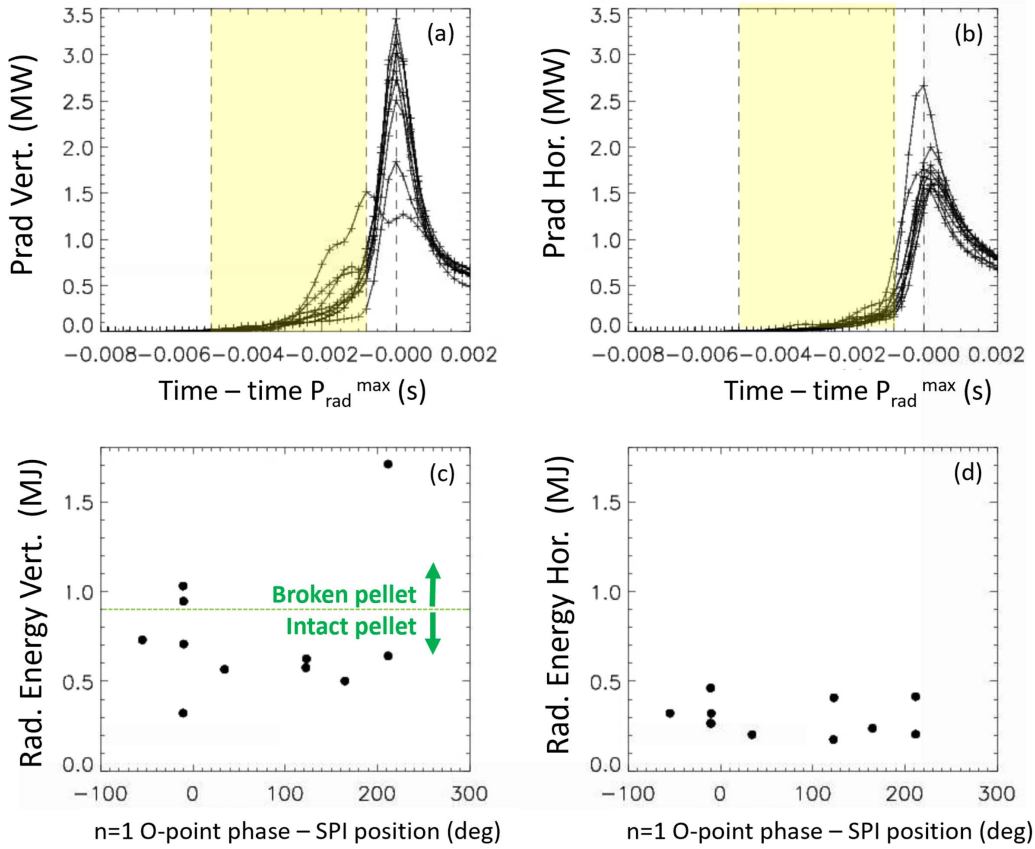

Figure 4. Time behavior of the (a) vertical and (b) horizontal radiated power with respect to the time of the maximum radiation and the corresponding (c) vertical and (d) horizontal radiation energy as a function of the toroidal $n = 1$ O-point location with respect to the SPI location. Data refers to the 20 MW NBI heated H-mode discharges with SPI pellet injection at 320 m s^{-1}.

of the gradual rise preceding the peak radiation, we calculated the radiated energy 4 ms before reaching the maximum radiated power. As shown in figure 4, this analysis enabled us to statistically differentiate between broken and intact pellets. The presence of a broken pellet is also confirmed by looking at the pellet brightness over time in the fast cameras. Indeed, in the fast camera images, it is possible to distinguish two groups of pellet shards trajectories, as depicted in panel (*l*).

(iii) #102547, reported on right panels of figure 3, represents the peculiar case where, the pellet is intact when passing the microwave cavity, as demonstrated by the presence of a single spike in the microwave cavity signal reported in panel (*p*). However, the radiated power, from both the vertical and the horizontal bolometry arrays has a quite broad envelope, as shown in panel (*q*) and two distinguishable groups of pellet shard trajectories can be traced in the fast cameras: a small shard starting at $t = 15.973$ and then the main one at $t = 15.975$ s as in panels (*r*) and (*s*), respectively. This evidence supports the premature pellet breakage before the shatter section.

An automatic procedure which checks the integrity of the pellets has been established considering bolometry data, and the results have been checked afterwards against microwave cavity and fast camera signals. Such automatic procedure consists in calculating over 4 ms the radiated energy from the vertical and the horizontal bolometry arrays, starting from 1 ms before the maximum radiated power, which corresponds to the yellow shaded regions shown in figures 4(a) and (b), respectively.

The analysis presented here is from data in the Hmode database utilizing only fast pellets, primarily impacted by broken pellets. As illustrated in figures 4(c), when the radiated energy from the vertical bolometry SPI pellet is suspected to be broken, making the corresponding radiation asymmetry factor defined in equation (1) unsuitable for TPF calculation. The signature of a broken pellet is present only in the vertical bolometry signal because this array is close to the SPI injector, while the horizontal one is far apart.

It is worth mentioning that once the timing of the pellet arrival in the chamber is known, a pellet integrity monitor can be designed based on the radiated energy, supplemented by microwave and fast camera data. This monitor can be useful to request a modification of the pellet injection sequence in case of degraded pellet injection, ensuring an effective mitigation action. However, this assumes that the pellet traveling time is not excessively long and that the amount of neon injection is optimized; otherwise, the current quench would be too short.

Once the pulses characterized by pellet breakage were identified and excluded, the radiation asymmetry factor was computed using equation (1). The resulting radiation asymmetry

Table 1. Parameters that have been identified by fitting equations (2) and (3) to the measured radiated asymmetries.

Database	$\lambda\varphi$(deg)	Δp	$\Delta\varphi$
Ohmic, 180 m s^{-1} pellet inj.	131	0.35	−27
14 MW NBI H mode, 180 m s^{-1} pellet inj.	135	0.22	−20
20 MW NBI H mode, 180 m s^{-1} pellet inj.	170	0.16	46
20 MW NBI H mode, 320 m s^{-1} pellet inj.	168.6	0.22	246

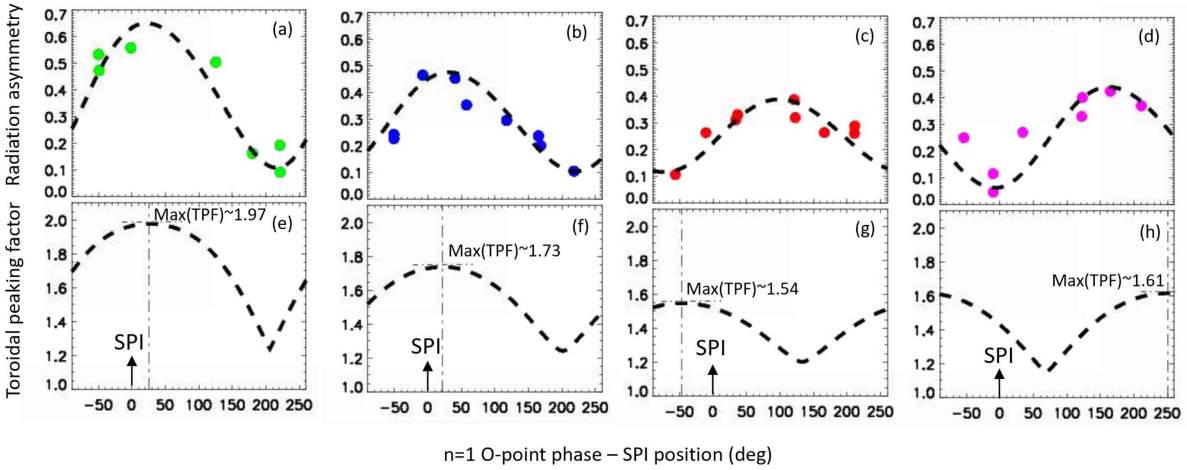

Figure 5. Radiation asymmetry factor taken at the time of the maximum radiation power as a function of the toroidal $n = 1$ O-point location with respect to the SPI location in (a) Ohmic discharges, (b) 2.3 MJ and (c) 3.2 MJ stored energy discharges with SPI pellet injection at 180 m s^{-1} and (d) 3.2 MJ stored energy H-mode discharges with SPI pellet injection at 320 m s^{-1} . The dashed line corresponds to the model fit, described in the text, using the experimental data. (e)–(h) Corresponding TPF toroidal distribution with respect to the SPI location deduced by the interpretative radiation model, described in the text and adopted in [6, 7].

data is presented in figures 5(a)–(c) for the Ohmic, the 13 and the 20 MW NBI heated databases, respectively. Across these datasets, the pellet injection velocity has been the same, around 180 m s^{-1} . It is worth noting that the data in panel (b) is the same as in [6] and is included here for completeness.

In figure 5(d), radiation asymmetry data is also presented for the 20 MW NBI H-mode scenario, but with a higher pellet injection, of about 320 m s^{-1}. This variation enabled us to study the impact of pellet injection velocity on the toroidal radiation distribution.

To compute the TPF, radiation asymmetry data has been analyzed based on certain assumptions regarding impurity density, $n_i(\varphi)$, and radiation distribution, $p_{\rm dis}(\varphi)$, functions, as follows [6, 7]:

$$n_i(\varphi) = n_{\rm i,0} \exp\left[-\left(\varphi - \Delta\varphi_{\rm inj}\right)/\lambda\phi\right]^2 \qquad (2)$$

$$p_{\rm dis}(\varphi) = 1 + \Delta p \cos\left(\varphi\, n = 1 - \Delta\varphi_{\rm inj} - \varphi\right) \qquad (3)$$

with φ varying from $-\pi$ to π and $\phi_{\rm inj}$ as the toroidal location of the SPI. The width of the impurity density distribution, $\lambda\phi$ the amplitude of the variation by the mode, Δp, and the phase offset $\Delta\varphi_{\rm inj}$ are free parameters that have been used to fit the model to the measured radiated asymmetries.

The product of the cosine and the Gaussian distributions and the averaged radiated power then gives the toroidally resolved radiated power, as

$$P_{\rm rad}(\varphi) = \langle P_{\rm rad}\rangle\, n_i(\varphi)\, p_{\rm dis}(\varphi) \qquad (4)$$

and the TPF for a given location of the O-phase of the $n = 1$ magnetic island φ_m is found using the formula of the radiation distribution:

$$\mathrm{TPF}(\varphi_m) = P_{\rm rad\,max}(\varphi_m) \,/\, \langle \mathrm{P_{rad}}\rangle. \qquad (5)$$

Using the fitted parameters $\lambda\phi$ Δp, and $\Delta\varphi_{\rm inj}$ reported in table 1 for each database, the toroidal distribution of the TPF has been reconstructed and the corresponding trend is illustrated in figures 5(e)–(h). Notably, the TPF trend presented in panel (f) is as in [6] and is included here for comparison.

The results obtained with the same pellet velocity, i.e. 180 m s^{-1}, suggest that the maximum of the TPF decreases with the plasma energy, as summarized in figure 6(a). The decreasing max TPF is favorable for thermal quench mitigation of plasma with higher stored energy, as the one envisaged in ITER.

It is worth reporting that ITER will have the capability to inject Ne/H pellets from several toroidal locations. Studies have shown [6] that this could reduce peak heat loads through a broader impurity distribution, provided that the timing of the different injections is optimized. This can help to reduce the TPF.

Note that the toroidal position of the maximum TPF for the various databases analyzed is close to the injection location, as shown in figure 5(b). This confirms that the asymmetric heat

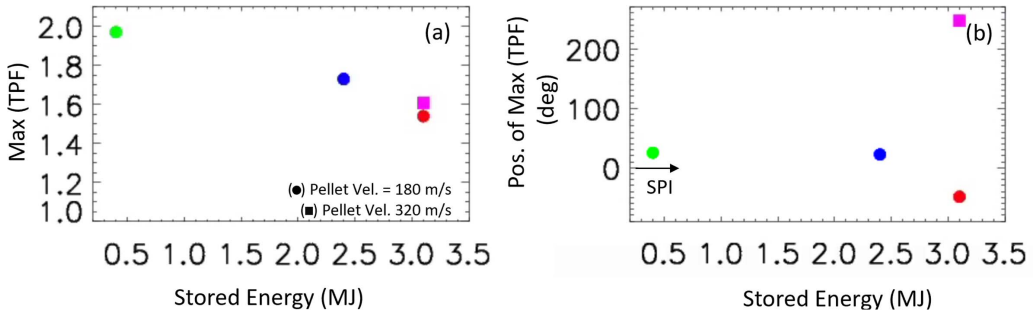

Figure 6. Stored energy as a function of (a) the maximum value of the toroidal peaking factor and (b) its toroidal position with respect to the SPI location. Different symbols have been used to distinguish the pellet velocity.

flux due to the $n = 1$ mode plays a role in driving the radiation asymmetry, in addition to the localized impurity source, consistently with [17].

However, when comparing the results obtained from the 20 MW H-mode scenario with faster pellet, it becomes apparent that there is a phase shift in the maximum TPF position between the 180 and the 320 m s^{-1} pellet injections.

Interestingly, for faster pellets the maximum TPF is found when the mode locks opposite to the injection location. This has also been observed in NIMROD simulations and was caused by heat flux emerging from the X-point of the magnetic island after the thermal quench [17] and in some DIII-D experiments [23]. At JET, the change in sector of the peak radiation feature is not consistent with the change in phase of the $n = 1$ mode, as in DIII-D.

Studies on the pellet injector trajectories, MHD modes, role of plasma rotation, complimented with JOREK [24] simulations and Emis3D analyses [25, 26] are ongoing to justify this physics insight and will be presented in a dedicated manuscript.

It is worth mentioning that during MGI experiments at DIII-D, a rotation effect on the peak radiation location has been observed [27]. The rotation in our JET experiments increases with higher stored energy and thus may have some role on the maximum TPF and the peak location relative to the SPI location. On ITER this may not be a large effect given the expected low rotation.

4. Conclusions

The successful exploitation of ITER will depend on establishing reliable and effective strategies to predict and avoid disruptions and as a final line of defense to mitigate disruptions.

During mitigated disruptions, the radiation release needs to be spread as uniform as possible to avoid local heat loads that exceed the melting limit of the SS components in front of the diagnostic ports.

In this context, dedicated experiments have been carried out at JET to quantify the radiation asymmetry during disruption mitigation with SPI in plasmas with various stored energies, achieved by scanning the NBI power.

The main result achieved within this study is that the toroidal peaking factor, a figure of merit which represents how the radiation distribution is toroidally concentrated, decreases with plasma energy and the maximum values is located at the injection for slow pellet injections (180 m s^{-1}).

Interestingly, for discharges with the same stored energy but with faster pellet injection (320 m s^{-1}), the maximum value of the toroidal peaking factor remains the same, but its phase is shifted opposite to the injector. It has been documented [28] that faster pellets have a very different fragmentation distribution from the slow pellets, and this could impact the spread and location of the ablation and the deposition of impurities in the plasma. Data and JOREK modelling analyses are ongoing to investigate this physical insight.

Towards ITER disruption mitigations, our results point to a decreasing TPF max with increasing thermal energy, which is in the favorable direction for ITER. In addition, ITER is planning to inject from several toroidal locations aiming at a better toroidal spread of the radiation during the thermal quench, which is also suggested by JOREK simulations [29].

Data availability statement

All data that support the findings of this study are included within the article (and any supplementary files).

Acknowledgments

The JET SPI experiments have been carried out as collaboration between EUROfusion and the ITER Organization. The JET SPI has received funding through the ITER Project. The views and opinions expressed herein do not necessarily reflect those of the ITER Organization.

ORCID iDs

L Piron https://orcid.org/0000-0002-7928-4661
M Lehnen https://orcid.org/0000-0001-6043-8803
M Kong https://orcid.org/0000-0002-2004-3513
S Silburn https://orcid.org/0000-0002-3111-5113
D Terranova https://orcid.org/0000-0001-9339-283X

References

[1] Lehnen M *et al* 2013 *Nucl. Fusion* **53** 093007
[2] Herfindal J L, Shiraki D, Baylor L R, Eidietis N W, Hollmann E M, Lasnier C J and Moyer R A 2019 *Nucl. Fusion* **59** 106034
[3] Snipes J A *et al* 2021 *Nucl. Fusion* **61** 106036
[4] Baylor L R *et al* 2021 *Nucl. Fusion* **61** 106001
[5] Lehnen M *et al Proc. 27th IAEA Fusion Energy Conf. (FEC 2018)* (*Gandhinagar, India*) pp EX/P7–12
[6] Jachmich S *et al* 2022 *Nucl. Fusion* **62** 026012
[7] Lehnen M, Gerasimov S N, Jachmich S, Koslowski H R, Kruezi U, Matthews G F, Mlynar J, Reux C and de Vries P C 2015 *Nucl. Fusion* **55** 123027
[8] Dibon M *et al* 2023 *Rev. Sci. Instrum.* **94** 043504
[9] Commaux N *et al* 2016 *Nucl. Fusion* **56** 046007
[10] Park S *et al* 2021 *Fusion Eng. Des.* **164** 112200
[11] Liang Y *et al* 2019 *Nucl. Fusion* **59** 112016
[12] Xu H B *et al* 2020 *Fusion Sci. Technol.* **76** 857–60
[13] Eidietis N W, Izzo V A, Commaux N, Hollmann E M and Shiraki D 2017 *Phys. Plasmas* **24** 102504
[14] Pitts R A *et al* 2015 *J. Nucl. Mater.* **463** 748–75
[15] Lehnen M *et al* 2015 *J. Nucl. Mater.* **463** 39–48
[16] Piron L *et al* 2023 *Fusion Eng. Des.* **197** 114069
[17] Izzo V A *et al* 2015 *Nucl. Fusion* **55** 073032
[18] Shiraki D, Commaux N, Baylor L R, Eidietis N W, Hollmann E M, Izzo V A, Moyer R A and Paz-Soldan C 2015 *Nucl. Fusion* **55** 073029
[19] Sørensen H *et al* 1990 *Rev. Sci. Instrum.* **61** 3464
[20] Lovell J, Reinke M L, Sheikh U A, Sweeney R, Puglia P, Carvalho P and Baylor L 2021 *Rev. Sci. Instrum.* **92** 023502
[21] Izzo V A *et al* 2013 *Phys. Plasmas* **20** 056107
[22] Olynyk G M *et al* 2013 *Nucl. Fusion* **53** 092001
[23] Sweeney R *et al* 2021 *Nucl. Fusion* **61** 066040
[24] Hoelzl M *et al* 2021 *Nucl. Fusion* **61** 065001
[25] Sweeney R 2020 *62nd APS DPP Annual Meeting* (available at: https://meetings.aps.org/Meeting/DPP20/Session/TI02)
[26] Stein-Lubrano B *et al* 2024 *Nucl. Fusion* **64** 036020
[27] Hollmann E M *et al* 2008 *Nucl. Fusion* **48** 115007
[28] Gebhart T E *et al* 2020 *Fusion Science and Technology* (American Nuclear Society)
[29] Hu D, Nardon E, Hoelzl M, Wieschollek F, Lehnen M, Huijsmans G T A, van Vugt D C, Kim S-H, (JET Contributors and JOREK Team) 2021 *Nucl. Fusion* **61** 026015